Available online at www.sciencedirect.com
SCIENCE DIRECT®
ELSEVIER
Earth and Planetary Science Letters 6853 (2003) 1–12
EPSL
www.elsevier.com/locate/epsl

Recent crustal deformation and the earthquake cycle along the Ecuador–Colombia subduction zone

Scott M. White *, Robert Trenkamp, James N. Kellogg

Department of Geological Sciences, 701 Sumter Street, University of South Carolina, Columbia, SC 29208, USA

Received 24 March 2003; received in revised form 15 September 2003; accepted 15 September 2003

Abstract

Recent results from Global Positioning System (GPS) measurements show deformation along the coast of Ecuador and Colombia that can be linked to the rupture zone of the earthquake in 1979. A 3D elastic boundary element model is used to simulate crustal deformation observed by GPS campaigns in 1991, 1994, 1996, and 1998. Deformation in Ecuador can be explained best by 50% apparent locking on the subduction interface. Although there have not been any historic large earthquakes ($M_w > 7$) south of the 1906 earthquake rupture zone, 50% apparent elastic locking is necessary to model the deformation observed there. In Colombia, only 30% apparent elastic locking is occurring along the subduction interface in the 1979 earthquake rupture zone (M_w 8.2), and no elastic locking is necessary to explain the crustal deformation observed at two GPS sites north of there. There is no evidence from seismicity or plate geometry that plate coupling on the subduction zone is reduced in Colombia. However, simple viscoelastic models suggest that the apparent reduction in elastic locking can be explained entirely by the response of a viscous upper mantle to the 1979 earthquake. These results suggest that elastic strain accumulation is occurring evenly throughout the study area, but postseismic relaxation masks the true total strain rate.

Keywords: Andes; subduction; plate coupling; postseismic relaxation; seismic locking

1. Introduction

Some of the greatest earthquakes in the 20th century and the greatest present earthquake hazard in South America occur in Ecuador and Colombia due to subduction of the Nazca plate [1] (Fig. 1). Rapid convergence at the Ecuador–Colombia Trench resulted in four large earthquakes ($M_w > 7.5$) in the 20th century [2,3]. This earthquake sequence is one of the best documented examples of the asperity model of earthquake rupture [2,4,5]. At the Colombia–Ecuador Trench, the Nazca plate subducts obliquely beneath South America at a convergence rate of 58 mm/a [6]. As a consequence of the oblique subduction, the entire northwest Andean area has broken away from stable South America, and is escaping northeastward as the North Andes Block [7]. The Nazca plate carries the aseismic Carnegie Ridge beneath Ecuador just to the south of the earthquake zone, locally deforming the subducting plate, and

* Corresponding author. Tel.: +1-803-777-6304; Fax: +1-803-777-6610.
E-mail address: swhite@geol.sc.edu (S.M. White).

0012-821X/03/$ – see front matter © 2003 Published by Elsevier B.V.
doi:10.1016/S0012-821X(03)00535-1

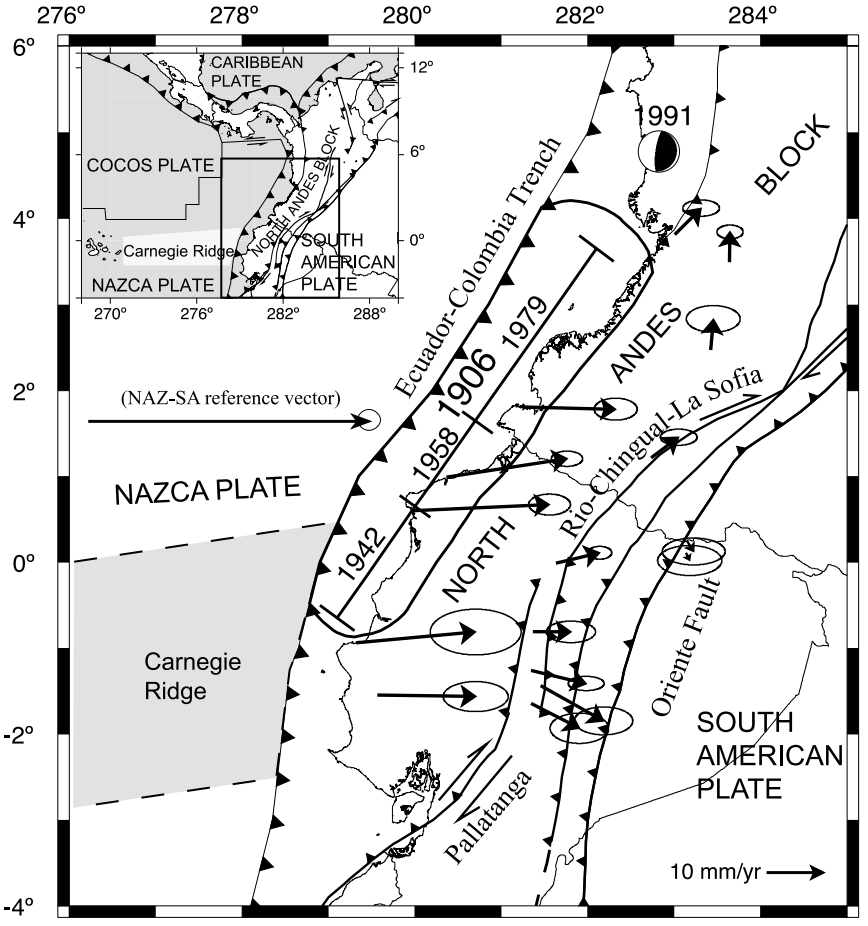

Fig. 1. Tectonic map of the major faults surrounding the North Andes Block. Regional tectonic setting is shown in the inset, with map area boxed. The CASA GPS horizontal velocity vectors relative to stable South America are shown with 1σ uncertainty ellipses [6]. The North Andes Block is bounded by the Ecuador–Colombia Trench, and the Pallatanga fault and the Rio-Chingual–La Sofia right-lateral fault system. The Carnegie Ridge (approximate extent shown with light shading) enters the Ecuador–Colombia Trench near the southern boundary of the North Andes Block. The approximate rupture zones of the 1906 earthquake and the subsequent 1942–1958–1979 earthquake sequence are indicated [2]. The focal mechanism for the 1991 earthquake is plotted over its approximate location [Harvard CMT catalog].

possibly increasing the coupling between the Nazca and South American plates [8].

The Central and South America (CASA) Global Positioning System (GPS) project was initiated in 1988 with goals including measuring the intraplate deformation in the northern Andes and the amount of aseismic convergence across the subduction zone [9]. Subsequent campaigns have determined crustal velocities and added sites to the original survey [6,10]. The CASA project results indicate highly variable rates of crustal deformation in Colombia and Ecuador (Fig. 1).

The relationship between the earthquake cycle and crustal deformation along subduction zones is beginning to be better understood, mainly by modeling recent GPS geodetic results. Geodetic observations suggest that great subduction zone earthquakes do not stop abruptly but rather steadily decay into slow slip down dip of the seismogenic zone. Postseismic subduction zone deformation involves both short-term afterslip on the fault plane and long-term viscoelastic relaxation of the lower crust/upper mantle [11–15]. In the first several months following an earthquake, on-

going slip on the rupture plane ('afterslip') and poroelastic effects may contribute a significant component of the GPS deformation in combination with the relaxation [14–18]. Klotz et al. [19] and Freymueller et al. [20] suggest that postseismic deformation continues for decades following great ($M_w > 8.5$) earthquakes. In this study, we examine the crustal deformation field observed by GPS surveys, and the effect of the sequence of 20th century earthquakes along the Ecuador–Colombia Subduction Zone (ECSZ).

We present 3D elastic half-space models to broadly explore spatial variations in the CASA GPS observations of the crustal deformation along the ECSZ, and a viscoelastic model to understand the postseismic crustal deformation attributable to individual earthquake events. Previous work modeling crustal deformation in this region has been limited to simple 2D elastic-slip models [6]. This 3D modeling allows us to pull together the spatial variability of seismic rupture in this area with a well-constrained earthquake cycle and a decadal-scale crustal deformation record from GPS geodesy to constrain spatial variations in the crustal deformation field related to individual earthquake rupture zones [2,4,5].

The amount of elastic locking on a fault indicates how much of the plate motion is being stored for release in future seismic (elastic) slip events versus how much aseismic slip occurs. We have opted to use the term 'apparent elastic locking' throughout this paper to describe the amount of elastic locking indicated by GPS data since the amount of true elastic locking on a fault may be obscured by postseismic relaxation or may be stored in small, fully (100%) locked patches between aseismically slipping zones. A denser network of continuous GPS receivers than currently exists would be necessary to differentiate between these scenarios.

2. Earthquake cycle of the Ecuador–Colombia Trench

In 1906, a great earthquake (M_w 8.8) ruptured a ~500 km long segment of the Ecuador–Colombia Trench [3]. Since that time, three other earthquakes have re-ruptured this same segment from south to north (Fig. 1). The first event, in 1942, was the least intense (M_w 7.6) followed by a larger event in 1958 (M_w 7.7) and the largest one in 1979 (M_w 8.2) [2,3]. The earthquakes following the 1906 event show no significant overlap between their rupture areas as defined by aftershock sequences [21]. However, the total seismic moment of the earthquakes after 1906 released only a small fraction of the energy of the 1906 event, leading to the speculation that another large earthquake ($M_w > 7.5$) had a >60% probability of occurring during the 1990s [1,22]. The fairly regular sequence of seismic events in the 20th century, interpreted as one of the best examples of the asperity model of earthquake rupture, plus the seismic hazard in this area, makes this an ideal region to study the crustal deformation associated with the earthquake cycle.

3. GPS data

We used a subset of the CASA GPS data from campaigns in 1991, 1994, 1996, and 1998 to look specifically at deformation in Ecuador and Colombia, where the sequence of great earthquakes occurred in the last century (Fig. 1). All data were transformed into the ITRF96 reference frame and velocity vectors were determined relative to stable South America. Details of the 1991 data processing can be found in Freymueller et al. [10] while Trenkamp et al. [6] describe processing details for subsequent campaigns. Only horizontal velocities were used in this study due to the large uncertainties associated with the vertical velocities. A complete list of GPS vectors for the CASA project can be found on-line (http://estrella.geol.sc.edu/~agl/CASA.htm) and in Trenkamp et al. [6].

4. Elastic boundary-element model attributes

A boundary element modeling code, 3d-def [23], was used to simulate the horizontal components of the GPS velocities along the ECSZ. Deformation is modeled as relative deformation in an elastic half-space due to strain accumulation

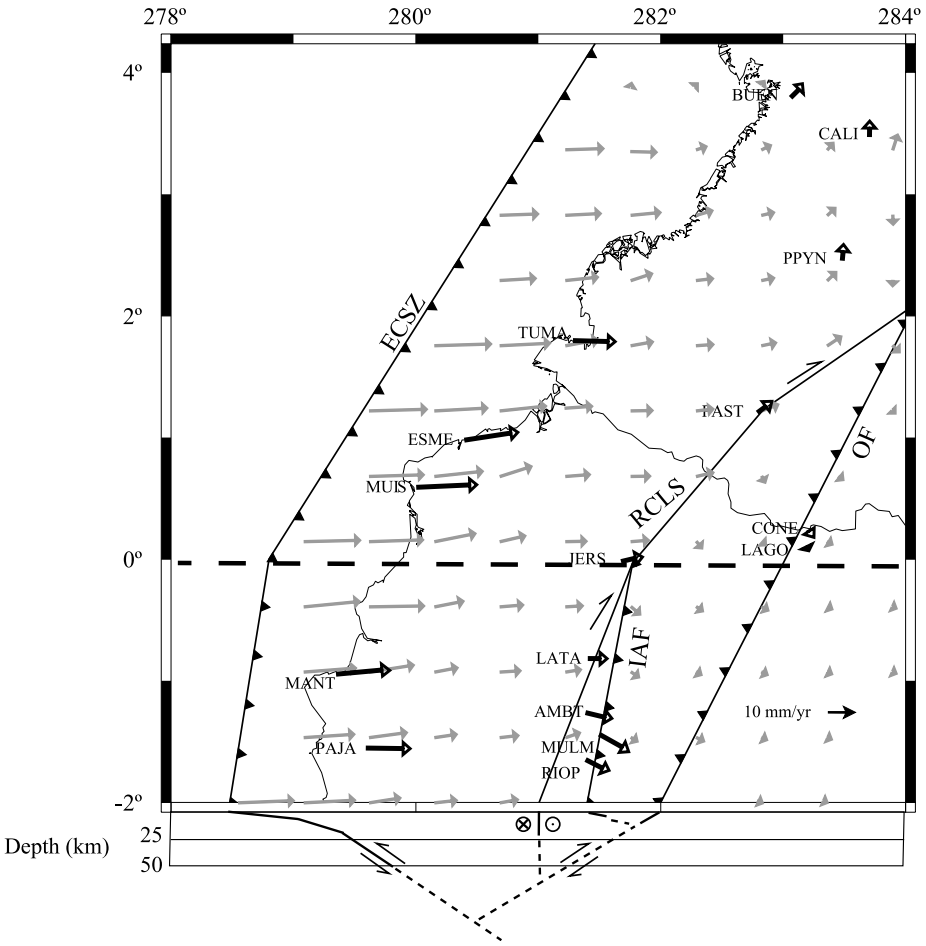

Fig. 2. Model setup showing simplified fault geometry in the Ecuador–Colombia region. Gray arrows show the horizontal vectors from the best-fit model (also in Fig. 5; see text for details). Black arrows show the CASA GPS horizontal vectors. The Ecuador–Colombia Subduction Zone (ECSZ), Rio-Chingual–La Sofia right-lateral faults (RCLS), Inter-Andean Fault (IAF), and Oriente Fault (OF) are shown with black lines. At the bottom, a cross-section through the model at −2° latitude is illustrated for the faults showing the variations in dip, the solid line shows the depth of locking, and the dashed line is the inferred continuation of the fault. The dashed line shows the location of the east–west 2D profile presented in Fig. 3.

imposed on a defined fault plane following the method of Savage [24]. This simple model assumes a uniform, perfectly elastic rock (Poisson's ratio = 0.25) within the half-space, and no significant topographic effects. These assumptions do not account for viscous deformation or Andean topographic effects at some of the inland sites located in the Andes mountains. Though it may seem that a homogeneous half-space model is inappropriately simple for the task of modeling the interaction of relatively stiff oceanic crust subducting beneath a more compliant continental crust, summarizing the complexities of slab dynamics and rheological variations by a set of boundary conditions on the slip interface can successfully model the large-scale behavior of the system [13,24]. These models are an appropriate way to examine which general processes may contribute to the spatial variations in GPS-observed deformation. We seek to understand how much locking along the ECSZ is required to account for the latitudinal changes in the GPS velocities, and how much slip is accommodated on the major right-lateral faults bounding the eastern side

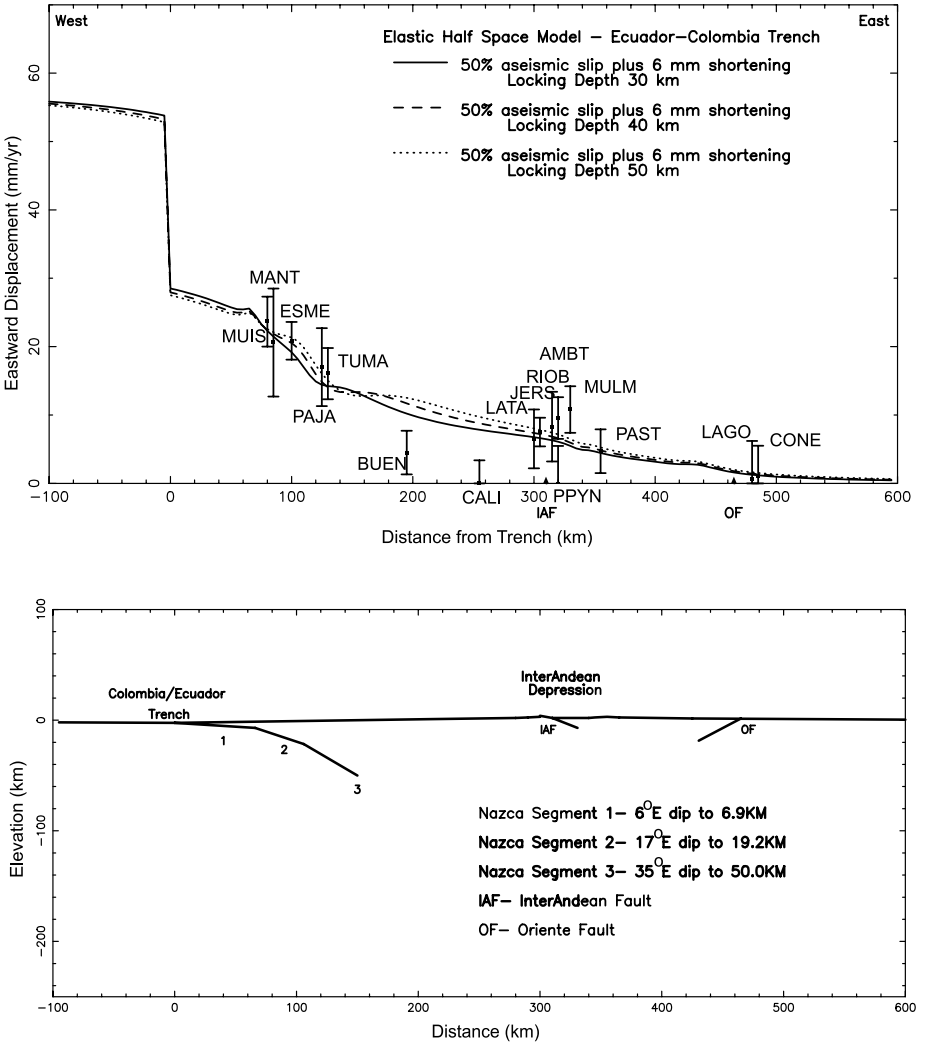

Fig. 3. Elastic half-space models compared to CASA GPS eastward velocities (dots) relative to stable South America with 1σ uncertainty ellipses. Only the depth of locking on the subduction zone interface is varied. All models use a convergence rate of 58.2 mm/a at the subduction zone interface, which is modeled as three segments with increasing down-dip angles. Shortening is modeled as 3 mm/a on the east-dipping IAF and 3 mm/a on a generalized west-dipping Oriente thrust fault (OF). Aseismic slip refers to that percentage of slip accommodated aseismically at the subduction zone. Location shown in Fig. 2. The range of the locking depths modeled produces similar results.

of the North Andes Block. The locations and geometry of these faults are constrained by previous geologic and seismic studies, and we consider these fixed for modeling purposes. We can then run simulations varying the amount of slip on each of the faults to best reproduce the CASA GPS observations.

The fault geometry in our model was derived from geological investigations of the major active faults bounding the North Andes Block (Figs. 1 and 2). The ECSZ was modeled as two segments with their dips constrained from seismicity [7,25,26]. Seismicity on the ECSZ indicates a maximum locking depth of 50 km [2]. This depth is within the range of values estimated for the depth of locking in the southern Andes [19,27]. A series of simulations show that varying the locking depth of the ECSZ from 30 to 50 km

does not change observed surface deformation significantly, as indicated in trench-normal 2D profile models (Fig. 3). Thus, we held the locking depth on the ECSZ constant at 50 km for all our models. This represents the maximum depth of elastic response on the subduction interface, which will also yield a minimum estimate of apparent elastic locking. Examination of Fig. 3 indicates that the main source of error is in the GPS observations and the uncertainties inherent in the elastic half-space model. We expect that variations of as much as 10% in the apparent elastic locking on the ECSZ, for any fixed set of model parameters, would produce essentially equally valid models within the uncertainty of our GPS data.

Shortening of the Andes by convergence in the Inter-Andean Valley may contribute to deformation within the North Andes Block, which we model as two discrete faults, the west-verging Inter-Andean Fault (IAF) and east-verging Oriente Fault (OF). The modeled IAF dips 30° east, strikes N10E, is locked to a depth of 10 km, and terminates at its intersection with the dextral shear zone in the north. The OF strikes N25E through the entire study area, dips 30° west, and is locked at a depth of 20 km. These depth estimates are consistent with studies of microseismicity in the area [28]. Dextral shear along the La Sofia–Rio-Chingual fault system accommodates the northeastward escape of the North Andes Block [7]. These dextral faults were modeled with three vertical segments of varying strike, each locked to a depth of 20 km.

Initial values for slip rates along the faults used for the models were taken from either geodetic measurements or geological estimates. Slip along the ECSZ is assumed to be equal to the 58 mm/a convergence rate between stable South America and the Galapagos Islands in the Nazca plate [6]. Other slip rates were estimated by offsets of rock units or morphological changes along the East Andean dextral shear faults, and slip generally increases from south to north. We assume slip on the dextral faults that average the geologically measured slip on the Rio-Chingual system of 8 mm/a, and the more northward La Sofia fault slipping at 12 mm/a [29,30]. Convergence on the IAF and OF are simulated with 3 mm/a shortening on each fault.

5. Results from elastic slip modeling

We simulated the surface deformation field observed by GPS measurements by varying the amount of apparent locking with the fault geometry held constant. We began by allowing uniform slip on each fault in the model using the initial slip rates described in the preceding section. We then examined the effects for: (1) convergence on the ECSZ, (2) shortening on the OF and IAF, and (3) dextral shear on the La Sofia–Rio-Chingual fault system. The elastic locking on the ECSZ was systematically varied by 20% intervals from 100% locking to 0% locking, both with and without shortening, and with and without dextral slip. The results from an illustrative subset of these simulations are illustrated by plotting the residuals, obtained by subtracting the GPS-observed horizontal velocity vector from model-derived vectors to find the best fit model (Fig. 4). We also calculated the chi-squared merit function for each simulation as:

$$\chi^2 = \frac{1}{n}\left(\sum^{n}\frac{(X_{\mathrm{mod}}-X_{\mathrm{GPS}})^2}{\sigma X^2_{\mathrm{GPS}}} + \sum^{n}\frac{Y_{\mathrm{mod}}-Y_{\mathrm{GPS}})^2}{\sigma Y^2_{\mathrm{GPS}}}\right)$$

where n is the number of data or vectors, X and Y are two orthogonal horizontal components of the model and GPS vectors as indicated in subscript, and σX and σY are one standard error of each component. Decreasing chi-squared values indicate a better agreement between model and observation.

Initial slip values calculated with 100% locking on each fault greatly overestimate the amount of eastward motion above the ECSZ (Fig. 4A). Dextral slip along the East Andean shear zone is required to explain the northward component of GPS vectors in the Andes. The geologically determined increase from 8 mm/a in the south to 12 mm/a in the north fits GPS-observed results within the observational uncertainty.

Reducing the apparent elastic locking on the ECSZ to 50% provides much better agreement between the model and observed GPS vectors,

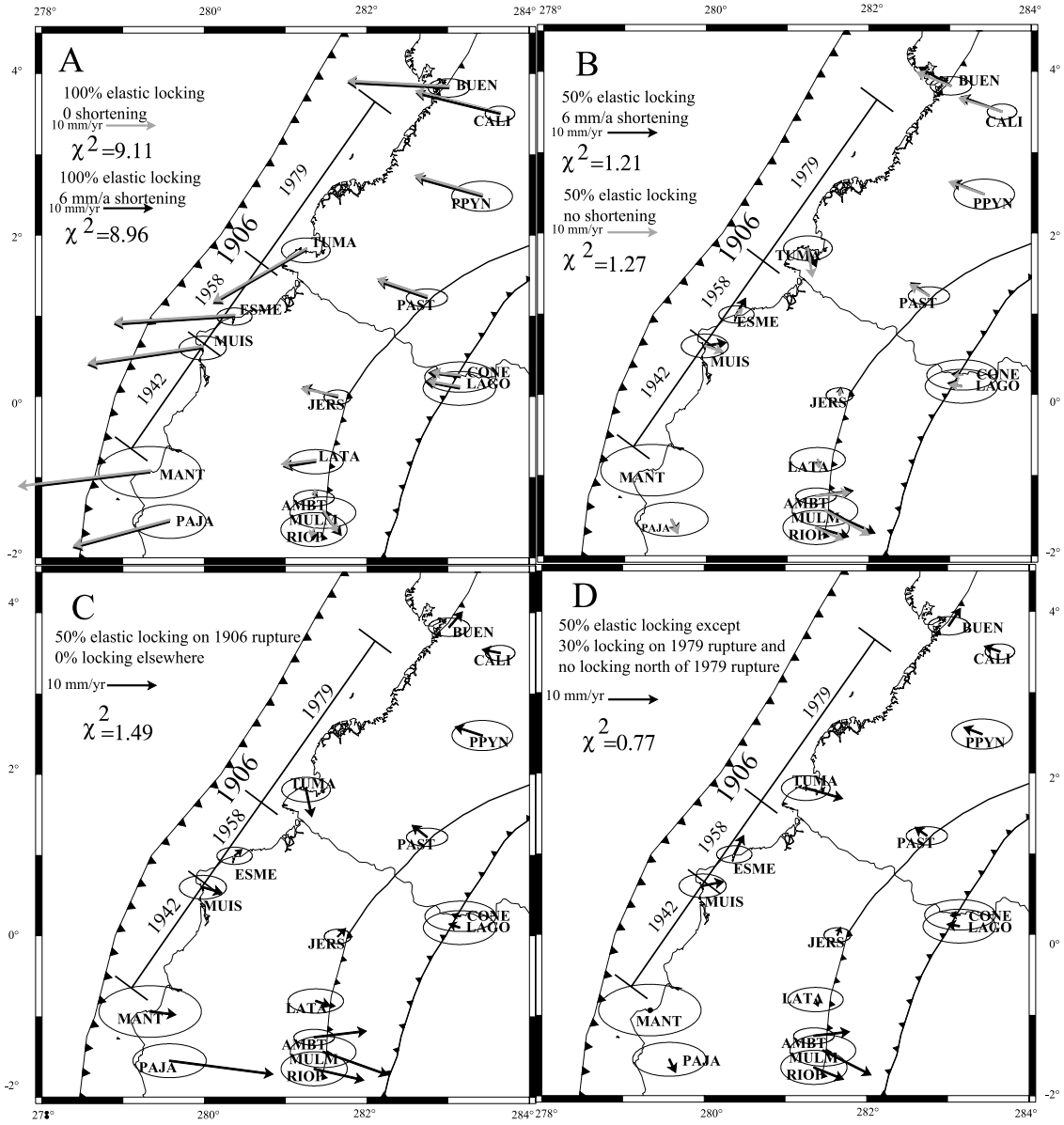

Fig. 4. Residuals from simulations varying locking on the ECSZ. The vectors on each map represent the misfit between the elastic-slip model and observed GPS velocity vectors calculated by subtracting the observed vector from the model vector. Black arrows indicate the residual, including a total 6 mm/a shortening on the Inter-Andean and Oriente faults and dextral shear on the Rio-Chingual–La Sofia faults. The chi-squared value relating the residual to the observational error for each simulation is given. Panel A shows uniform 100% locking. Panel B shows uniform 50% locking. In panels A and B, light arrows indicate the residual for simulations with no shortening on the Inter-Andean and Oriente faults. Panel C shows the residuals from 50% locking on only the 1906 earthquake rupture zone. Panel D shows the residuals from 30% locking on the 1979 earthquake rupture zone, no locking on the short segment to the north of it, and 50% on the rest of the ECSZ. The chi-squared value <1.0 for the simulation in panel D indicates that the residuals are less than the observational error of the GPS measurements.

reducing the X^2 values from ~9 to ~1 (Fig. 4B). This agrees with the results from a trench-perpendicular profile 2D model by Trenkamp et al. [6]. In contrast to the results in Trenkamp et al. [6], we find that including Andean shortening fails to improve the agreement between model and observed velocity vectors. The change in X^2 values associated with 6 mm/a shortening in the Andes is <0.1 (Fig. 4A,B). The impact of Andean shortening is greater in the 2D model of Trenkamp et al. [6] than our 3D model because the 2D model did not take into account the finite length of the IAF and the eastward motion on the dextral shear zone. GPS velocities in the Inter-Andean Valley indicate that deformation is complex, possibly including some oblique component on the IAF, or multiple fault strands through the valley. Simplifications to the fault geometry in constructing the model may cause some of the disagreement in the Inter-Andean Valley, where shortening and dextral shear both occur and slip rates are not well constrained. Local deformation associated with volcanic activity is beyond the regional focus of this study, but warrants further investigation. In this study, we maintain a simple model in southern Ecuador and accept some error at GPS sites AMBT, MULM, and RIOP in exchange for minimizing error at MANT and PAJA (Fig. 4).

At this point, it is apparent that uniform locking along the ECSZ cannot adequately model the differences in eastward displacement at CASA GPS sites in the northern and southern part of our study area simultaneously. No major change in the trench geometry occurs at this location; the Carnegie Ridge intersects the trench farther south [8]. However, large trench earthquakes occurred in this part of the study area, including the northern part of the 1906 rupture, the entire 1979 rupture, and a smaller 1991 event (Fig. 1).

No large historical earthquakes have occurred south of the 1906 rupture zone, suggesting that locking might be minimal there. However, limiting elastic locking to the 1906 earthquake rupture zone produces a significant underestimate of the eastward velocities south of the 1906 rupture, suggesting that elastic strain accumulation is taking place in southern Ecuador despite the lack of historic earthquakes (Fig. 4C).

We developed a series of models to account for the low GPS velocities seen along coastal Colombia by varying the amount of locking in the rupture zones of recent earthquakes in 1942, 1958, and 1979. Varying locking on the rupture planes of the 1942 and 1958 earthquakes only increases the X^2 value, so these models are not shown. We find that 50% apparent elastic locking on the ECSZ south of the 1979 rupture zone, 30% apparent elastic locking in the 1979 rupture zone, and no apparent locking north of the 1979 rupture zone provides the closest match for all of the observed GPS velocities and is the only model with a X^2 less than 1.0 (Fig. 4D). The reduced apparent elastic locking in Colombia brings the simulated velocities within the 1σ error ellipse of GPS observations at CALI, PPYN, and PAST at the expense of a slight underestimation of the eastward component at TUMA (Fig. 4D). Although the model still underestimates the magnitude of the vector at BUEN, the azimuth of this vector is now correct.

Our elastic slip models show significantly reduced locking associated with the rupture zone of the 1979 earthquake (Figs. 2 and 4D). Given that the elastic models work as well here as they do farther to the south along the Nazca–South America plate margin, the apparent elastic locking is substantially reduced in our study area relative to other well-studied parts of the South America subduction system (e.g. [19,27]). The reduced apparent elastic locking associated with the rupture zones of these moderately large earthquakes may be caused by either: (1) reduced seismic coupling on the ECSZ, or (2) postseismic afterslip and viscoelastic relaxation of the lower crust/upper mantle. Coupling should be a long-term process, unchanging over millenia, related to some physical properties of the fault rather than the earthquake cycle. In contrast, deformation in the form of afterslip and viscoelastic relaxation occurs over periods of time corresponding to the seismic cycle [12,13].

6. Viscoelastic relaxation from the 1979 earthquake

To evaluate whether viscoelastic relaxation

could be a factor in the reduced apparent elastic locking associated with the 1979 earthquake rupture zone, we modeled the expected postseismic deformation using the VISCO1D model [18] (http://www.geology.ucdavis.edu/~pollitz). VISCO1D calculates the gravitational viscoelastic response in a spherical, stratified Earth caused by a fault in the top elastic layer. We used the parameters given by Kanamori and McNally [2] for the fault plane geometry and average coseismic displacement of the 1979 event. The assumed viscosity structure of the lower crust and upper mantle strongly affects the model results, but is very poorly constrained. We used the viscosity structure derived from measurement of forearc uplift after the great 1960 Chile earthquake, assuming viscous effects in the upper asthenosphere at depths of 40–150 km [31]. The density and elastic moduli of each Earth layer in the model were taken from the PREM values [32]. We tested models with upper asthenospheric viscosities ranging from 10^{19} to 10^{21} Pa s with a fixed lower mantle viscosity of 10^{21} Pa s, and elastic crust to explore a wide range of values for the viscosity structure. The further complication of a viscoelastic lower crust in the Andes may produce an even greater relaxation effect, especially for the more inland sites, but lateral variations in crustal structure are beyond the capabilities of VISCO1D and the data currently available to constrain viscosity structure in the region.

The lowest-viscosity models that we tested produce a viscoelastic relaxation from the 1979 earthquake that is able to account for the apparent reduction in elastic locking (Fig. 5). A uniform 50% elastic locking along the entire ECSZ masked by viscoelastic relaxation from the 1979 earthquake due to a 10^{19} Pa s viscosity asthenosphere provides an equally good fit to the GPS data as the best-fit variation in the elastic locking models. This provides compelling evidence that viscoelastic relaxation can account for the observed latitudinal variations in elastic locking.

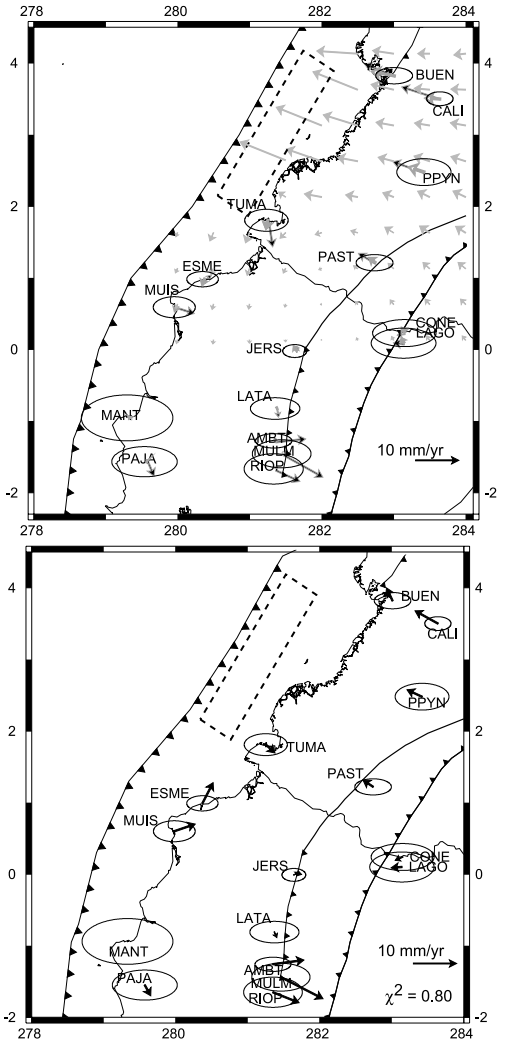

Fig. 5. Simulated crustal velocities produced by viscoelastic relaxation after the 1979 earthquake in a spherical, layered Earth with an upper mantle viscosity of 10^{19} Pa s. The fault plane of the 1979 earthquake used in the model is shown as a dashed rectangle. On the top panel, the light-colored arrows show the viscoelastic deformation field, dark open arrows show the viscoelastic deformation at each CASA GPS site, and dark filled arrows show the residual from uniform 50% elastic along the entire subduction interface (Fig. 4B). The bottom panel shows the residual left after subtracting the viscoelastic reponse from the residual from uniform 50% elastic locking shown in the top panel. The ellipses are 1σ uncertainty ellipses from the original CASA GPS velocity vectors. The X^2 values for this model indicate that the viscoelastic response from the 1979 earthquake satisfies the data as well as varying elastic locking along the fault.

7. Discussion

The reduction in GPS velocities in Colombia

relative to Ecuador requires some mechanism to reduce the apparent elastic strain accumulating in Colombia. The reduction in apparent elastic strain may be a true reduction in plate coupling or viscoelastic rebound that masks strain accumulation. We find it mechanically unlikely that there would be reduced coupling on the Colombian part of the ECSZ where several large historic earthquakes have occurred. Geological conditions along the subduction interface are not generally thought to change spatially through southern Colombia. The Carnegie Ridge intersects the trench several hundred kilometers to the south of this area, although the extent of its influence on the Nazca plate is not well known. Earthquake hypocenters and abundance suggest uniform seismic coupling through this area as well [8]. However, much more sediment is found in the trench off Colombia.

The 1979 (M_w 8.2) earthquake was much smaller in magnitude than the great earthquakes where postseismic deformation has been observed for several decades [19,20,33,34]. However, CASA GPS measurements used in this study began only 12 years after the 1979 earthquake. Postseismic deformation has been noted in GPS observations a few years after earthquakes of this magnitude (e.g. [35]). Viscoelastic models of the expected postseismic deformation based on the earthquake source from the 1979 event show that postseismic effects related to a low-viscosity upper mantle can explain the apparent reduction in coupling along the ECSZ in Colombia (Fig. 5).

The first GPS campaign in this study occurred prior to the 1991 (M_w 7.2) earthquake (Fig. 1). Estimating the coseismic slip from this event indicates that no effects should be seen within our study area. The maximum effect from the 1991 earthquake is felt at BUEN, but amounts to <1 m/a change in the total velocity. The coseismic effect drops by an order of magnitude or more for the other sites.

Results from our elastic half-space boundary-element modeling of surface displacements and viscoelastic relaxation from the 1979 earthquake are consistent with 50% apparent elastic locking on the ECSZ throughout the entire study area. The southern boundary of the 1906 earthquake rupture zone inferred by Kanamori and McNally [2] seems to have no effect on the elastic locking. Since large earthquakes are absent from the historical record south of the 1906 rupture zone, elastic strain stored in southern Ecuador either may be released in earthquakes with a very long recurrence interval or by aseismic events such as 'slow earthquakes'. Our result of 50% elastic locking means that only half of the total plate motion is stored for eventual release in earthquake (elastic) events. Although partial locking or aseismic creep has proven useful for modeling interseismic surface deformation, it makes little sense physically, given what is known about plate contact friction [15]. Partial locking may occur uniformly over the fault plane, or it is possible that part of the fault plane may be fully (100%) locked while other parts are slipping aseismically, akin to the asperity model of earthquakes.

Elastic strain accumulated on the ECSZ by convergence of the Nazca and South American plates must be released in earthquake events at the trench. The slip released in the 1942–1958–1979 sequence of very large earthquakes re-rupturing the 1906 rupture zone probably released most of the seismic slip being stored on the ECSZ. Kanamori and McNally [2] estimated the slip resulting from each of these earthquakes. These estimated values of seismic slip average approximately 67% of the cumulative convergence at the trench since 1906 (Fig. 6). Only a very small real difference between the 50% locking estimated from GPS and 67% locking estimated from seismic slip might be explained by ongoing postseismic viscoelastic rebound from the 1906 earthquake. Viscoelastic relaxation models of the 1906 earthquake using parameters given by Kanamori and McNally [2] produce deformation rates of <1 mm/a for the same Earth stratification model used for the 1979 earthquake. These numbers are insignificant, but larger values for viscoelastic rebound would tend to increase the elastic locking estimate derived from GPS. The large uncertainties associated with both estimates of elastic strain do not rule out that all of the elastic locking is being released as elastic slip (Fig. 6). In either case, it seems apparent that a large part of the convergence seems to be taking

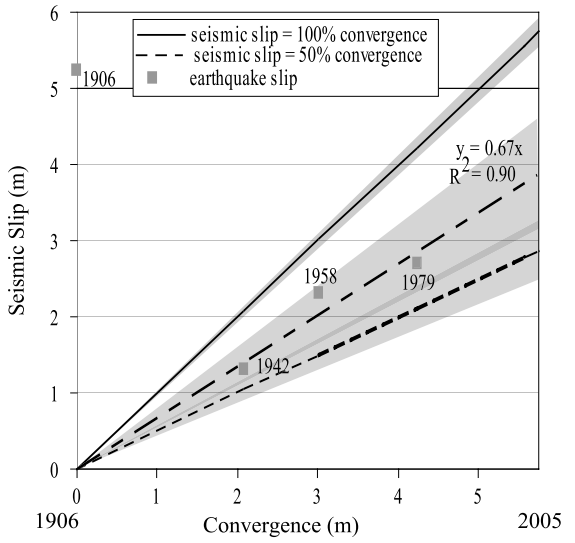

Fig. 6. Seismic slip on the Ecuador–Colombia Trench since 1906 plotted against a Nazca–South America convergence rate of 58 mm/a [6]. Estimates of seismic slip for each earthquake are from Kanamori and McNally [2]. The solid line indicates the seismic slip necessary to release all of the convergence with 1σ error envelope (shaded area). The short dashed line is the estimate of seismic slip necessary to release 50% of the total accumulated convergence. A linear least-squares fit to the estimates of seismic slip from earthquakes is shown with a long dashed line (error envelope for this regression indicated by the shaded area), and suggests that these earthquakes have been releasing ~67% of the total accumulated convergence.

place aseismically. This may occur through steady aseismic creep, by aseismic afterslip, or by 'slow earthquakes'. Detecting aseismic events in action in order to differentiate between these mechanisms requires a dense network of continuous GPS stations.

8. Conclusion

Our modeling shows that the deformation along the ECSZ can be related to the earthquake cycle. In particular, viscoelastic relaxation associated with the recent earthquake in 1979 (M_w 8.2) can explain the reduction in apparent elastic locking in Colombia. That is, 50% elastic locking along the entire subduction zone fits the observed crustal deformation when the expected viscoelastic relaxation from the 1979 earthquake is subtracted from the total vector field. However, so little viscoelastic response from the 1906 event is observed that ongoing postseismic relaxation cannot account for the low apparent elastic locking along the entire margin. The apparent elastic locking observed south of the 1906 rupture zone indicates that elastic strain is building in a region where no great earthquakes have been recorded.

Acknowledgements

The CASA project was supported by NSF Grants EAR-8617485, EAR-8904657, and NASA. The GPS observations were made with assistance from INGEOMINAS in Colombia and Instituto Geografico Militar in Ecuador. We thank Edmundo Norabuena and Tim Dixon for constructive advice on earlier versions of this manuscript. Reviews by T. Masterlark and an anonymous reviewer greatly improved the manuscript.*[SK]*

References

[1] S.P. Nishenko, Circum-Pacific Seismic Potential 1989-1999, U.S. Geol. Surv., 1989, 126 pp.
[2] H. Kanamori, K.C. McNally, Variable rupture mode of the subduction zone along the Ecuador-Colombia coast, Bull. Seism. Soc. Am. 72 (1982) 1241–1253.
[3] J.A. Kelleher, Rupture zones of large South American earthquakes and some predictions, J. Geophys. Res. 77 (1972) 2087–2103.
[4] J.L. Swenson, S.L. Beck, Historical 1942 Ecuador and 1942 Peru subduction earthquakes and earthquake cycles along Colombia-Ecuador and Peru subduction segments, PAGEOPH 146 (1996) 67–101.
[5] S.L. Beck, L.J. Ruff, The rupture process of the Great 1979 Colombia earthquake: Evidence for the asperity model, J. Geophys. Res. 89 (1984) 9281–9291.
[6] R. Trenkamp, J.N. Kellogg, J.T. Freymueller, H. Mora, Wide plate margin deformation, southern Central America and northwestern South America, CASA GPS observations, J.S. Am. Earth Sci. 15 (2002) 157–171.
[7] J.N. Kellogg, V. Vega, Tectonic development of Panama, Costa Rica, and the Colombian Andes: Constraints from Global Positioning System geodetic studies and gravity, in: P. Mann (Ed.), Geologic and Tectonic Development of the Caribbean Plate Boundary in Southern Central America, Geol. Soc. Am. Spec. Pap. 295 (1995) 159–200.
[8] M.-A. Gutscher, J. Malavieille, S. Lallemand, J.-Y. Collot, Tectonic segmentation of the North Andean margin:

Impact of the Carnegie Ridge collision, Earth Planet. Sci. Lett. 168 (1999) 255–270.
[9] J.N. Kellogg, T.H. Dixon, Central and South America GPS geodesy; CASA Uno, Geophys. Res. Lett. 17 (1990) 195–198.
[10] J.T. Freymueller, J.N. Kellogg, V. Vega, Plate motions in the North Andean region, J. Geophys. Res. 98 (1993) 21853–21863.
[11] A. Nur, G. Mavko, Postseismic elastic rebound, Science 183 (1974) 204–206.
[12] S.C. Cohen, Postseismic deformation due to subcrustal viscoelastic relaxation following dip-slip earthquakes, J. Geophys. Res. 89 (1984) 4538–4544.
[13] L.J. Ruff, Stress on the seismogenic and deep creep plate interface during the earthquake cycle in subduction zones, Earth Planets Space 53 (2001) 307–320.
[14] T. Masterlark, C. DeMets, H.F. Wang, O. Sanchez, J. Stock, Homogeneous vs heterogeneous subduction zone models: coseismic and postseismic deformation, Geophys. Res. Lett. 28 (2001) 4047–4050.
[15] T. Melbourne, F. Webb, J. Stock, C. Reigber, Rapid postseismic transients in subduction zones from continuous GPS, J. Geophys. Res. 107 (2002) E1–E10.
[16] T. Nakano, K. Hirahara, GPS observations of postseismic deformation for the 1995 Hyogo-ken Nanbu earthquake, Japan, Geophys. Res. Lett. 24 (1997) 503–506.
[17] X. LePichon, S. Mazzotti, P. Henry, M. Hashimoto, Deformation of the Japanese Islands and seismic coupling: an interpretation based on GSI permanent GPS observations, Geophys. J. Int. 134 (1998) 501–514.
[18] F.F. Pollitz, R. Burgmann, P. Segall, Joint estimation of afterslip rate and postseismic relaxation following the 1989 Loma Prieta Earthquake, J. Geophys. Res. 103 (1998) 26975–26992.
[19] J. Klotz, G. Kahzaradze, D. Angermann, C. Reigber, R. Perdomo, O. Cifuentes, Earthquake cycle dominates contemporary crustal deformation in Central and Southern Andes, Earth Planet. Sci. Lett. 193 (2001) 437–446.
[20] J.T. Freymueller, S.C. Cohen, H.J. Fletcher, Spatial variations in present-day deformation, Kenai Peninsula, Alaska, and their implications, J. Geophys. Res. 105 (2000) 8079–8101.
[21] C. Mendoza, J.W. Dewey, Seismicity associated with the great Colombia-Ecuador earthquakes of 1942, 1958, and 1979; implications for barrier models of earthquake rupture, Bull. Seism. Soc. Am. 74 (1984) 577–593.
[22] E. Papadimitriou, Long-term earthquake prediction along the western coast of South and Central America based on a time predictable model, Pure Appl. Geophys. 140 (1993) 301–316.
[23] J. Gomberg, M. Ellis, Topography and tectonics of the central New Madrid seismic zone: Results of numerical experiments using a three-dimensional boundary-element program, J. Geophys. Res. 99 (1994) 20299–20310.
[24] J.C. Savage, A dislocation model of strain accumulation and release at a subduction zone, J. Geophys. Res. 88 (1983) 4984–4996.
[25] R.O. Meissner, E.R. Fleuh, F. Stibane, E. Berg, Dynamics of the active plate boundary in Southwest Colombia according to recent geophysical measurements, Tectonophysics 35 (1976) 115–136.
[26] W.D. Pennington, Subduction of the eastern Panama Basin and seismotectonics of northwestern South America, J. Geophys. Res. 86 (1981) 10753–10804.
[27] B.W. Tichelaar, L.J. Ruff, Seismic coupling along the Chilean subduction zone, J. Geophys. Res. 96 (1991) 11997–12022.
[28] G. Suarez, P. Molnar, C.B. Burchfiel, Seismicity, fault plane solutions, depth of faulting and active tectonics of the Andes of Peru, Ecuador, and southern Colombia, J. Geophys. Res. 88 (1983) 10403–10428.
[29] A. Tibaldi, J.R. Leon, Morphometry of late Pleistocene-Holocene faulting and volcanotectonic relationship in the southern Andes of Colombia, Tectonics 19 (2000) 358–377.
[30] F. Ego, M. Sebrier, A. Lavenu, H. Yepes, A. Egues, Quaternary state of stress in the Northern Andes and the restraining bend model for the Ecuadorian Andes, Tectonophysics 259 (1996) 101–116.
[31] A. Piersanti, Postseismic deformation in Chile: Constraints on the asthenospheric viscosity, Geophys. Res. Lett. 26 (1999) 3157–3160.
[32] A.M. Dziewonski, D.L. Anderson, Preliminary reference earth model (PREM), Phys. Earth Planet. Inter. 25 (1981) 297–356.
[33] K. Wang, J. He, H. Dragert, T. James, Three-dimensional viscoelastic interseismic deformation model for the Cascadia subduction zone, Earth Planets Space 53 (2001) 295–306.
[34] S.J. Kenner, P. Segall, Postseismic deformation following the 1906 San Francisco earthquake, J. Geophys. Res. 105 (2000) 13195–13209.
[35] A. Piersanti, C. Nostro, F. Riguzzi, Active displacement field in the Suez-Sinai area: the role of postseismic deformation, Earth Planet. Sci. Lett. 193 (2001) 13–23.